Helicity amplitudes and Regge behavior for simple planar hadron amplitudes

C. Edward Jones and J. Uschersohn
Department of Physics and Astronomy, University of Nebraska—Lincoln, Lincoln, Nebraska 68588-0111
(Received 18 March 1985)

Helicity amplitudes for the simplest zero-entropy hadron amplitudes in topological particle theory are constructed. The kinematic singularities and the Regge asymptotic behavior of such amplitudes are studied in detail. The importance and effects of planar but nonzero-entropy corrections, which are expected to bring the zero-entropy amplitudes into reasonable agreement with the physical world, are discussed.

I. INTRODUCTION

Experience over a number of years with hadron scattering amplitudes—particularly, with various forms of dual resonance models—has indicated the physical importance of planar amplitudes.[1] The approximate exchange degeneracy of observed Regge trajectories is one such indication of the dominance of planar contributions.[1]

Topological particle theory[2] (TPT), which gives a fully relativistic theory of quark-constituted hadrons, has as its basic approximation planar zero-entropy amplitudes. Other planar contributions involving "chiral" and "color" switches are expected to modify the zero-entropy approximation in an important way.[3] It is expected that, just as earlier,[1] the dominant planar contributions should provide a reasonable approximation to the physical world in the case of hadron processes.

To set the stage for calculating the general planar contribution, we examine here the properties and the Regge behavior of zero-entropy helicity amplitudes. As in earlier work, the helicity amplitudes are very convenient for studying Regge behavior and thus for examining the asymptotic bounds on amplitudes.

We begin by showing how kinematic singularities arise in the zero-entropy helicity amplitudes. Then we study the Regge behavior of these amplitudes. At the zero-entropy level there is only one stable particle of mass m_0 and five degenerate elementary particles having mass m_0 but different spins.[4] Correspondingly, there are five parallel, nonlinear Regge trajectories separated by a spacing of $\frac{1}{2}$. We indicate that the bilinear unitarity-type self-consistency constraint[5] does not suffice to ensure that the zero-entropy helicity amplitudes satisfy the Froissart bound. Higher-order planar corrections must accomplish this. Further, we shall see that the zero-entropy Regge trajectories do not possess the ranking which is observed physically. Again we indicate the expected role of higher-order planar corrections in breaking the above mass degeneracy and reordering the trajectories.

II. ZERO-ENTROPY HELICITY AMPLITUDES

A zero-entropy amplitude is represented graphically by quark and diquark lines which have a planar structure consisting of untwisted quark lines. An example is shown in Fig. 1. If in the graph in Fig. 1 the lower part consists of incoming particles and the upper part outgoing particles, the process represented is just meson-baryon scattering. The small arrows adjacent to the quark lines called the patch structure determine the spin dependence.[6] A quark line for which the adjacent small arrow agrees in direction with the quark line direction is called an orthoquark. If the adjacent small arrow disagrees in direction with the quark line direction the quark is called a paraquark.

An orthoquark has a spin dependence arising from a scalar product of two two-component spinors with dotted indices—upper dotted indices being associated with the tail of the quark line and lower dotted indices being associated with the head of the quark line. A paraquark line involves scalar products of spinors with undotted indices—lower undotted indices being associated with the tail of the quark line and upper undotted indices being associated with the head of the quark line.

As an example the spin dependence associated with the left-most quark line in Fig. 1 is the scalar product[7]

$$n_{\dot{\alpha}}(v_D,\phi_D)\eta^{\dot{\alpha}}(v_A,\phi_A)\ , \tag{2.1}$$

where v_D and v_A are the four-vector velocities for particles D and A and ϕ_D and ϕ_A are two-component rest

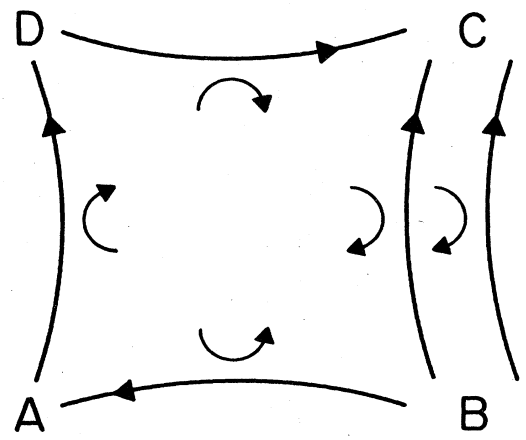

FIG. 1. Example of zero-entropy amplitude.

frame spin states for the out-quark and in-quark. Had the left-most quark been a paraquark the spin dependence would have been the scalar product[5]

$$\eta^{\alpha}(v_D,\phi_D)\eta_{\alpha}(v_A,\phi_A)\ . \tag{2.2}$$

The complete zero-entropy amplitude entails a product of factors of the form (2.1) or (2.2) for each quark line together with a multiplicative Lorentz-invariant scalar function $f(p_A,p_B,p_C,p_D)$ (Refs. 5 and 7).

The spinors in (2.1) and (2.2) can be written as boosts applied to rest-frame spin states.[5,7] For example,

$$\eta^{\dot{\alpha}}(v,\phi)=\exp\left[-\lambda\frac{\hat{\mathbf{v}}\cdot\boldsymbol{\sigma}}{2}\right]\phi\ , \tag{2.3}$$

$$\mathbf{p}=m\hat{\mathbf{v}}\sinh\lambda\ ,$$

where we shall conventionally take $\lambda>0$ and thus $\hat{\mathbf{v}}$ is the direction of the three-momentum $\mathbf{p}$.

We now wish to introduce helicity states and then construct center-of-mass helicity amplitudes for four-particle amplitudes of the general type shown in Fig. 4 where $A+B\to D+C$. It is convenient to adopt the more or less standard convention for helicity states, namely,

$$\eta^{\pm}(v,\hat{\mathbf{n}}(\theta,\psi))=R(\psi,\theta,-\psi)B_z(\lambda)\phi_{\pm}\ , \tag{2.4}$$

where $\eta^{\pm}(v,\hat{\mathbf{n}}(\theta,\psi))$ are $\pm$ helicity states for the momentum direction $\hat{\mathbf{n}}(\theta,\psi)$ and $\phi_{\pm}$ are rest-frame spin states with a z spin projection of $\pm\frac{1}{2}$. $B_z(\lambda)$ is a boost along the z direction ($\lambda>0$) and $R(\psi,\theta,-\psi)$ is a rotation with the parameters corresponding to the three Euler angles. Equation (2.4) is a general expression and we have suppressed labels indicating whether $\eta^{\pm}$ is an in- or out-state and whether its indices are upper or lower, dotted or undotted. The detailed form of R, B, and $\phi_{\pm}$ will, of course, depend upon these properties. For example, for an in-state with upper dotted indices and positive helicity (2.4) will take the form

$$\eta^{\dot{\alpha}(+)}_{\text{in}}(v,\hat{\mathbf{n}})=e^{-i\psi\sigma_3/2}e^{-i\theta\sigma_2/2}e^{i\psi\sigma_3/2}e^{-\lambda\sigma_3/2}\begin{bmatrix}1\\0\end{bmatrix}$$

$$=e^{-\lambda/2}\begin{bmatrix}\cos\theta/2\\ e^{i\psi}\sin\theta/2\end{bmatrix}\ . \tag{2.5}$$

A distinct advantage of the conventions we have used in (2.4) is that if we wish to consider a helicity state moving in the opposite direction (i.e., $\hat{\mathbf{n}}\to-\hat{\mathbf{n}}$), the form of that state written in terms of θ and ψ will be the same whether $\psi<\pi$ or $\psi>\pi$.

To find the form of the negative helicity state in the example above we simply replace the rest-frame spinor $\binom{1}{0}$ by $\binom{0}{1}$ and find

$$\eta^{\dot{\alpha}(-)}_{\text{in}}(v,\hat{\mathbf{n}})=e^{\lambda/2}\begin{bmatrix}-e^{-i\psi}\sin\theta/2\\ \cos\theta/2\end{bmatrix}\ . \tag{2.6}$$

The states (2.5) and (2.6) correspond to incoming orthoquarks. Incoming paraquark states are spinors with lower undotted indices and have the same form as (2.5) and (2.6) except that the sign of λ in the exponent is reversed. This turns out to be a general rule: paraquark or paraantiquark states can be found by simply changing the sign of λ in the corresponding orthoquark and ortho-antiquark states. So for simplicity we shall restrict our discussion and examples to orthoquark and ortho-antiquark states.

The outgoing states corresponding to (2.5) and (2.6) have lower dotted indices and have the form

$$\eta^{(+)}_{\dot{\alpha}\ \text{out}}(v,\hat{\mathbf{n}})=e^{\lambda/2}\begin{bmatrix}\cos\theta/2\\ e^{-i\psi}\sin\theta/2\end{bmatrix}\ , \tag{2.7}$$

$$\eta^{(-)}_{\dot{\alpha}\ \text{out}}(v,\hat{\mathbf{n}})=e^{-\lambda/2}\begin{bmatrix}-e^{i\psi}\sin\theta/2\\ \cos\theta/2\end{bmatrix}\ . \tag{2.8}$$

For incoming ortho-antiquarks we must use lower undotted indices. The positive-helicity state is given by

$$\eta^{(+)}_{\dot{\alpha}\ \text{in}}(v,\hat{\mathbf{n}})=e^{i\psi\sigma_3/2}e^{-i\theta\sigma_2/2}e^{-i\psi\sigma_3/2}e^{\lambda\sigma_3/2}\begin{bmatrix}0\\1\end{bmatrix}$$

$$=e^{-\lambda/2}\begin{bmatrix}-e^{i\psi}\sin\theta/2\\ \cos\theta/2\end{bmatrix}\ . \tag{2.9}$$

The negative-helicity state for an incoming ortho-antiquark is obtained by replacing the rest-frame spinor $\binom{0}{1}$ in (2.9) with the spinor $\binom{1}{0}$, which gives

$$\eta^{(-)}_{\dot{\alpha}\ \text{in}}(v,\hat{\mathbf{n}})=e^{\lambda/2}\begin{bmatrix}\cos\theta/2\\ e^{-i\psi}\sin\theta/2\end{bmatrix}\ . \tag{2.10}$$

The outgoing states corresponding to (2.9) and (2.10) have upper dotted indices and have the form

$$\eta^{\dot{\alpha}(+)}_{\text{out}}(v,\hat{\mathbf{n}})=e^{\lambda/2}\begin{bmatrix}-e^{-i\psi}\sin\theta/2\\ \cos\theta/2\end{bmatrix}\ , \tag{2.11}$$

$$\eta^{\dot{\alpha}(-)}_{\text{out}}(v,\hat{\mathbf{n}})=e^{-\lambda/2}\begin{bmatrix}\cos\theta/2\\ e^{i\psi}\sin\theta/2\end{bmatrix}\ . \tag{2.12}$$

TABLE I. Helicity states for orthoquarks and antiquarks with momentum direction $\hat{\mathbf{n}}(\theta,\phi)$. $s=\sin\theta/2$, $c=\cos\theta/2$.

	Quark		Antiquark	
	+	−	+	−
In	$e^{-\lambda/2}\begin{bmatrix}c\\ e^{i\psi_S}\end{bmatrix}$	$e^{\lambda/2}\begin{bmatrix}-e^{-i\psi_S}\\ c\end{bmatrix}$	$e^{-\lambda/2}\begin{bmatrix}-e^{+i\psi_S}\\ c\end{bmatrix}$	$e^{\lambda/2}\begin{bmatrix}c\\ e^{-i\psi_S}\end{bmatrix}$
Out	$e^{\lambda/2}\begin{bmatrix}c\\ e^{-i\psi_S}\end{bmatrix}$	$e^{-\lambda/2}\begin{bmatrix}-e^{i\psi_S}\\ c\end{bmatrix}$	$e^{\lambda/2}\begin{bmatrix}-e^{-i\psi_S}\\ c\end{bmatrix}$	$e^{-\lambda/2}\begin{bmatrix}c\\ e^{i\psi_S}\end{bmatrix}$

TABLE II. Helicity states for orthoquarks and antiquarks with momentum direction $-\hat{\mathbf{n}}(\theta,\phi)$. $s=\sin\theta/2$, $c=\cos\theta/2$.

	Quark		Antiquark	
	+	−	+	−
In	$e^{-\lambda/2}\begin{bmatrix} s \\ -e^{i\psi_C} \end{bmatrix}$	$e^{\lambda/2}\begin{bmatrix} e^{-i\psi_C} \\ s \end{bmatrix}$	$e^{-\lambda/2}\begin{bmatrix} +e^{+i\psi_C} \\ s \end{bmatrix}$	$e^{\lambda/2}\begin{bmatrix} s \\ -e^{-i\psi_C} \end{bmatrix}$
Out	$e^{\lambda/2}\begin{bmatrix} s \\ -e^{-i\psi_C} \end{bmatrix}$	$e^{-\lambda/2}\begin{bmatrix} e^{+i\psi_C} \\ s \end{bmatrix}$	$e^{\lambda/2}\begin{bmatrix} e^{-i\psi_C} \\ s \end{bmatrix}$	$e^{-\lambda/2}\begin{bmatrix} s \\ -e^{+i\psi_C} \end{bmatrix}$

We have given here the complete set of spin states for orthoquarks and ortho-antiquarks. To obtain the corresponding states for paraquarks and para-antiquarks we simply (i) change the sign of λ in (2.5)—(2.12), and (ii) make all indices undotted and raise lower indices and lower upper indices in (2.5)—(2.12).

The results of this section are summarized in Table I. Again, if the sign of λ is everywhere reversed in Table I the spin states for paraquarks and para-antiquarks will result.

Since in the succeeding sections, we shall use the helicity states in Table I in the center of mass of 2 particle $\to$2 particle amplitudes of the type shown in Fig. 1, we have recorded in Table II the corresponding helicity states for the momentum direction $-\hat{\mathbf{n}}(\theta,\psi)$. Table II is derived from Table I by making the transformation:

$$\theta\to\pi-\theta\,,\qquad \psi\to\psi\pm\pi\,. \tag{2.13}$$

III. KINEMATIC SINGULARITIES OF HELICITY AMPLITUDES

We shall now verify that the kinematic singularities of the zero-entropy helicity amplitudes are of the expected form.[8] We assume a scattering amplitude of the general type shown in Fig. 1 corresponding to the process $A+B\to D+C$, although we shall also consider more general quark structures with either single quarks or diquarks connecting particles A, B, C, and D. We work in the center-of-mass frame and assume particle A to be moving along the positive z direction. We assume particle D emerges in the x-z plane and thus take $\psi=0$, with θ the scattering angle as shown in Fig. 2.

The helicity amplitude we consider can be written

$$T^{z_A z_B z_D z_C}_{\mu_A\mu_B\mu_D\mu_C}(s,\cos\theta)\,, \tag{3.1}$$

where the $\mu_A,\ldots,\mu_C$ are particle helicities and are determined by summing the helicities of the constituent quarks and antiquarks. The superscripts $z_A,\ldots,z_C$ designate the particular spin patch structure—i.e., which quarks are orthoquarks and which quarks are paraquarks. Due to rotational invariance the helicity amplitudes (3.1) should have kinematic zeros of the form[8]

$$T(s,\cos\theta)\sim(\sin\theta/2)^{|\mu_1-\mu_2|}(\cos\theta/2)^{|\mu_1+\mu_2|}\,,\qquad \mu_1=\mu_A-\mu_B\,,\qquad \mu_2=\mu_D-\mu_C\,. \tag{3.2}$$

Helicity amplitudes of the form (3.1) can be written[9]

$$T^{z_A,\ldots,z_C}_{\mu_A,\ldots,\mu_C}(s,\cos\theta)=\Gamma S^{z_A,\ldots,z_C} f(s,\cos\theta)\,, \tag{3.3}$$

where Γ is a phase factor discussed fully in Refs. 5 and 9. $S^{z_A,\ldots,z_C}$ is the spin structure factor which simply consists of pairs of Lorentz-invariant spin factors for each quark line of the type (3.1) for each quark line in the diagram and f is a Lorentz-invariant scalar function. Although the right-hand side of (3.3) is valid for any type of spin states, by inserting the helicity states from Tables I and II into the spin structure factor $S^{z_A,\ldots,z_C}$ we generate helicity amplitudes.

We first establish a general rule for horizontal quark lines occurring either at the top or the bottom of zero-entropy amplitudes of the type we are considering (Fig. 1). Such horizontal quark lines correspond to either incoming or outgoing quark-antiquark associated with opposite mo-

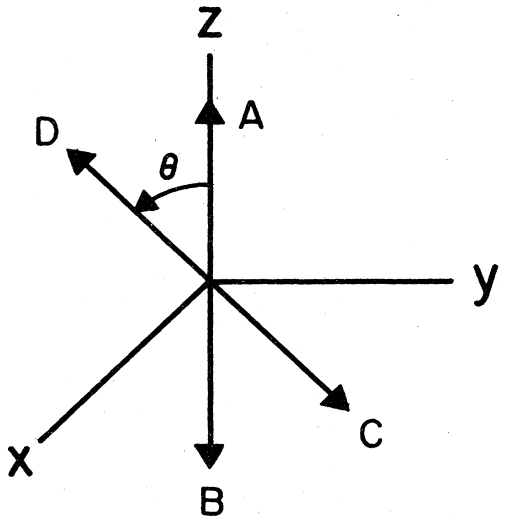

FIG. 2. Momentum diagram for process $A+B\to C+D$.

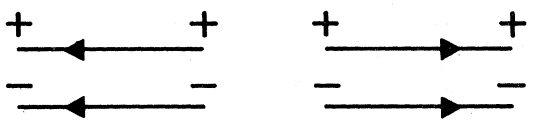

FIG. 3. Nonvanishing horizontal-quark-line contributions.

menta since we are in the center of mass. The spin-dependence of such lines is one factor in $S^{z_A,\ldots,z_C}$ of the general form (2.1) applied to a horizontal quark line using helicity spinors from Tables I and II. We find that such quark lines give a zero contribution if the helicity is flipped and a nonzero contribution only when the helicity of the quark and antiquark are the same. These nonzero contributions are indicated in Fig. 3. Furthermore, there is no θ dependence coming from spinor factors for the horizontal quark lines in Fig. 3.

It is thus clear that the kinematic singularities (3.2) must arise from the dependence on the spinor factors in $S^{z_A,\ldots,z_C}$ coming from the vertical quark lines connecting initial to final states. How this can result in the singularity structure (3.2) is not at first obvious since the θ dependence of each vertical quark line is independent of the helicity values of the other quark lines, yet the behavior (3.2) gives a θ behavior which involves a correlation of the helicity states on the left- and right-hand side of the amplitude diagram.

To see how this works out we give the general rules deduced from Tables I and II for calculating the θ dependence of vertical quark lines. The rules are as follows: all vertical quark lines (connecting incoming and outgoing states) give a behavior $\cos\theta/2$ if the helicity does not flip between the head and tail of the quark line and a behavior $\sin\theta/2$ if the helicity does flip. These results are indicated in Fig. 4. We emphasize that these results about the θ dependence apply equally to orthoquark and paraquark lines.

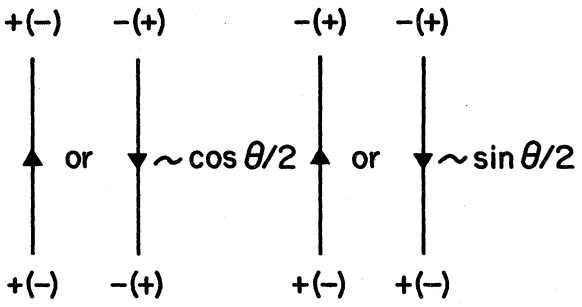

FIG. 4. The θ behavior of vertical quark lines.

It is, of course, convenient to use the quark helicity states as a basis in forming the particle helicity states of which the quarks are constituents. The helicity of the particle state is then just the sum of the constituent quark helicities since at zero entropy all quark states are boosted from rest with a velocity corresponding to that of the particle.

From the general results in this section as displayed in Figs. 3 and 4, we can immediately deduce the kinematic zeros of the zero-entropy helicity amplitudes to be as follows:

$$T^{z_A,\ldots,z_C}_{\mu_A,\ldots,\mu_C}(s,\cos\theta)\sim\left[\sin\frac{\theta}{2}\right]^{\sum_V|\mu_{AV}-\mu_{DV}|+\sum_V|\mu_{BV}-\mu_{CV}|}\left[\cos\frac{\theta}{2}\right]^{\sum_V|\mu_{AV}+\mu_{DV}|+\sum_V|\mu_{BV}+\mu_{CV}|}, \tag{3.4}$$

where $\sum_V$ indicates a summation over the helicities of the vertical quark lines. The required kinematic zeros are those indicated in (3.2), which when written in terms of the vertical quark helicity variables become (bearing in mind the results embodied in Fig. 3)

$$(T)_{\text{required}}\sim\left[\sin\frac{\theta}{2}\right]^{\sum_V|(\mu_{AV}-\mu_{DV})-(\mu_{BV}-\mu_{CV})|}\left[\cos\frac{\theta}{2}\right]^{\sum_V|(\mu_{AV}+\mu_{DV})-(\mu_{BV}+\mu_{CV})|}. \tag{3.5}$$

We see that the zeros of (3.3) and (3.4) do not, in general, exactly agree. The form of the zeros in (3.5) can be written somewhat more compactly as

$$(T)_{\text{required}}\sim(1-z)^{n_1}(1+z)^{n_2},\quad z=\cos\theta\,, \tag{3.6}$$

where n_1 and n_2 are non-negative and are either both integers or both half integers. The form of the zeros of the actual zero-entropy amplitude (3.4) can be written in the form:

$$(T)_{\text{zero entropy}}\sim(1-z)^{n_1'}(1+z)^{n_2'}\,, \tag{3.7}$$

where n_1' and n_2' have the same restrictions as those given above for n_1 and n_2. Comparing (3.5) [and (3.4)] we see that the quantities $(n_1'-n_1)$ and $(n_2'-n_2)$ may be either zero or a positive integer. Thus the zero-entropy helicity amplitudes have all the kinematics zeros and branch points required but may, in addition, have extra zeros in $(1+z)$ or $(1-z)$. However, no kinematic branch points exist in the z variable for the zero-entropy amplitudes beyond those indicated in (3.2) or (3.5).

IV. REGGE BEHAVIOR OF HELICITY AMPLITUDES

In this section, we shall investigate the Regge behavior of the zero-entropy helicity amplitudes. The helicity amplitudes have the virtue of possessing the asymptotic behavior of true J-plane Regge poles. This situation is to be contrasted with, e.g., the case of kinematic-singularity-free amplitudes whose asymptotic behavior is displaced

from that given by the J-plane poles.

From the form of the zero-entropy helicity amplitudes (3.3) we shall show that all the Regge trajectories are parallel displacements of the trajectories found in the scalar function f. The factorized spin dependence shown in (3.3) assures that stable elementary particles occurring at the zero-entropy level all have the same degenerate mass m_0.[4]

As a first step we examine in the s channel the asymptotic behavior of the helicity amplitude (3.1) for fixed s and large $\cos\theta$. This is an unphysical region but it indicates most directly the form of the asymptotic behavior as related to the J-plane poles. This is because (3.1) has the expansion (suppressing spin-patch-structure labels)

$$T_{\mu_A\mu_B\mu_D\mu_C}(s,\cos\theta)=\sum_{J=M}^{\infty}(2J+1)\times T^J_{\mu_A\mu_B\mu_D\mu_C}(s)d^J_{\mu_1\mu_2}(\theta)\,, \tag{4.1}$$

where M is the larger of $|\mu_1|$ and $|\mu_2|$. A Regge pole at $J=\alpha$ in the T^J amplitude in (4.1) gives rise to the asymptotic behavior $(\cos\theta)^\alpha$ independent of the particular values of μ_1 and μ_2.

Assuming the presence of a leading Regge trajectory $\alpha_0(s)$ in the scalar amplitude f of (3.3) we deduce a leading asymptotic behavior of the form

$$f(s,\cos\theta)\to(\cos\theta)^{\alpha_0(s)}\,. \tag{4.2}$$

Now we consider the asymptotic behavior of the spin structure factor $S^{z_A,\ldots,z_C}$ in (3.3) in order to determine the Regge behavior for the zero-entropy helicity amplitudes. We recall from the discussion regarding Fig. 3 that horizontal quark lines in $S^{z_A,\ldots,z_C}$ have no θ dependence. Further, from Fig. 4 we have that the behavior of each vertical quark line is either $\sin\theta/2$ or $\cos\theta/2$. So, in general, the zero-entropy helicity amplitude has the asymptotic behavior

$$T_{\mu_A\mu_B\mu_D\mu_C}(s,\cos\theta)\to(\cos\theta)^{\alpha_0(s)+n/2}\,, \tag{4.3}$$

where n is the number of vertical quark lines in the zero-entropy amplitude. The possible values of n for zero-entropy amplitudes and the corresponding Regge poles are as follows:

$n=2$, meson Regge pole,

$n=3$, baryon Regge pole,

$n=4$, baryonium Regge pole.

The highest-spin stable particle in each case is as follows. The meson trajectory has a stable spin-1 particle on it, the baryon trajectory a stable spin-$\frac{3}{2}$ particle, and the baryonium trajectory a stable spin-2 particle.

We shall now see that certain combinations of zero-entropy amplitudes with definite spin for the external particles will also generate asymptotic behavior corresponding to $n=0$ and $n=1$ in (4.3). These cases correspond to Regge trajectories whose highest spin stable particles are a spin-zero meson and a spin-$\frac{1}{2}$ baryon, respectively.

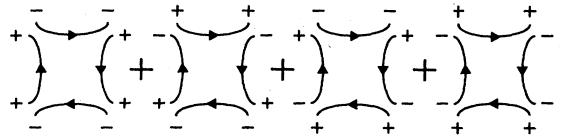

FIG. 5. Sum of amplitudes corresponding to scattering of spin-zero mesons.

We consider the sum of meson amplitudes shown in Fig. 5. The + and − denote helicity states and the sum shown gives an amplitude (up to a normalization constant) where all external mesons are spinless. It may be verified that this sum of amplitudes in Fig. 5 has no θ dependence if all quarks have the same patch structure (either ortho or para). Thus $n=0$ in (4.3). A similar type sum can be made involving a diquark in place of a single quark in one of the vertical positions leading to $n=1$ in (4.3). (In the latter case an amplitude is formed in which all the external states are spin zero when one of the quarks in the diquarks is absent.) We also note the following facts: (i) If one horizontal line in Fig. 5 has a different patch structure than the other three, then we still have $n=0$ in (4.3). (ii) If either or both vertical quark lines in Fig. 5 have opposite patch structure to the horizontal quark lines, again $n=1$ in (4.3).

In Fig. 6 are shown the five Regge trajectories that will be present at the zero-entropy level. Each trajectory gives the leading Regge behavior for some combination of zero-entropy amplitudes. The lowest-lying trajectory in Fig. 6 occurs as the leading trajectory in the scalar function f. The $s=0$ intercepts are not known although they are, in principle, determined by the zero-entropy bootstrap problem[10] which determines $\alpha_0(s)$. However, no particles or tachyons exist below m_0^2 so if trajectories pass through physical values for $s<m_0^2$, the residues will vanish. As we shall discuss, it is not inconsistent at the zero-entropy level to have trajectories lying above one at $s=0$. Also we mention that the flavor dependence of zero-entropy amplitudes completely factorizes [like the spin structure factor in (3.3)] and there is complete flavor symmetry.

The Regge behavior we have discussed so far and have used in determining the Regge trajectories has been in the unphysical region $(\cos\theta)\to\infty$. Ordinarily one would have to invoke the crossing properties[8] of helicity amplitudes in

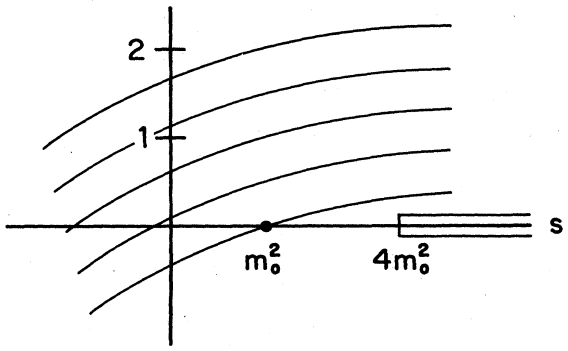

FIG. 6. Leading Regge trajectories at zero-entropy level.

order to determine the exact form of the Regge behavior in a physical region such as $s\to\infty$, t fixed. However, in the case of zero-entropy amplitudes we can determine this behavior directly through the use of Tables I and II and from the fact that

$$f(s,\cos\theta) \underset{\substack{s\to\infty \\ t \text{ fixed}}}{\longrightarrow} s^{\alpha(t)} , \tag{4.4}$$

where t is the momentum-transfer in the s channel.

First we note that at high energy the boost parameter and λ are related by

$$s \underset{\lambda\to\infty}{\longrightarrow} 4m_0{}^2 e^{2\lambda} . \tag{4.5}$$

Also at high energy, we have the relation between $\cos\theta$ and t

$$\cos\theta \underset{s\to\infty}{\longrightarrow} 1+\frac{2t}{s} . \tag{4.6}$$

From these two relations (4.5) and (4.6) we can conclude immediately that all vertical quark lines contribute a leading asymptotic behavior in s of order unity or less. In fact, the results can be summarized by saying all vertical quark lines give an asymptotic s behavior of order unity except that in the case of orthoquarks

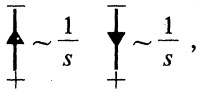

(4.7)

and in the case of paraquarks

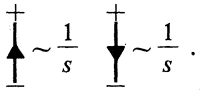

(4.8)

Thus any promotion of the Regge behavior from that of f given by (4.4) is determined by the horizontal (or exchanged) quark lines as one would expect. As mentioned earlier the horizontal quark lines do not allow helicity flip. The contribution of these horizontal lines for various cases is shown in Fig. 7 for orthoquarks. The lower part of Fig. 7 gives the results for incoming quark-antiquark states and the upper part gives the results for outgoing quark-antiquark states. For the case of paraquarks the sign of λ is reversed in Fig. 7. Since $e^{\lambda}\to\sqrt{s}$ as $s\to\infty$, we see that each exchanged quark line is capable of promoting the asymptotic Regge behavior by a maximum amount of a factor $\sqrt{s}$. This is consistent with our earlier results in this section such as (4.3) and Fig. 6 where Regge behavior was determined in the crossed channel. Here we have been able to determine the Regge behavior in the physical region without resorting to the use of helicity crossing matrices.

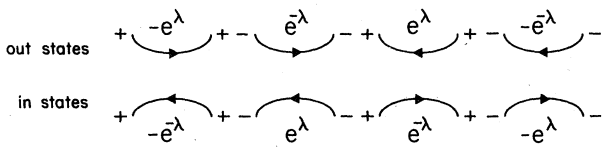

FIG. 7. The λ behavior of horizontal quark lines.

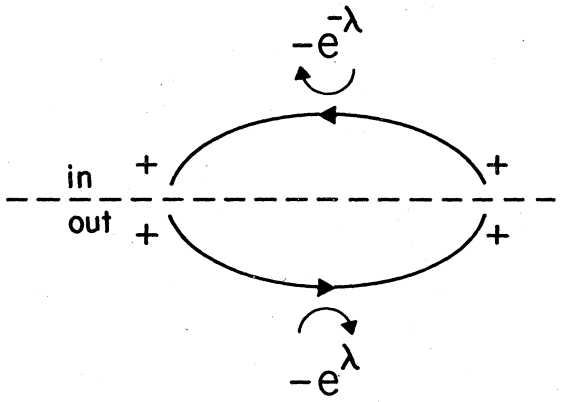

FIG. 8. Closed loop involving quark lines with same patch structure.

For the results embodied in Fig. 7 we can also understand why Regge trajectories which exceed unity in the forward direction [$\alpha(0)>1$] and, hence violate the Froissart bound are not inconsistent with the nonlinear bootstrap condition for zero-entropy amplitudes. As has been discussed previously the zero-entropy amplitudes are not unitary although they do obey a discontinuity equation which would be equivalent to the unitarity condition if the individual zero-entropy amplitudes were Hermitian analytic. However the individual zero-entropy amplitudes are not Hermitian analytic so they are not unitary. Nonzero-entropy corrections are required to enforce unitarity. From Fig. 7 we see that any quark loop contained in the intermediate state for a zero-entropy discontinuity relation will always involve a power of both e^{λ} and $e^{-\lambda}$ as long as the two quark lines making up the loop have the same patch structure, (i.e., are both ortho or para). This is illustrated in Fig. 8. Thus the bilinear constraint on the amplitude does not limit the Regge power and therefore the Froissart bound is not obeyed.

However, as higher-order corrections are included of the type shown in Fig. 9, which corresponds to a chiral switch (the quark line in one half of the loop being ortho and in the other half being para), the bilinear constraints will eventually force agreement with the Froissart bound.

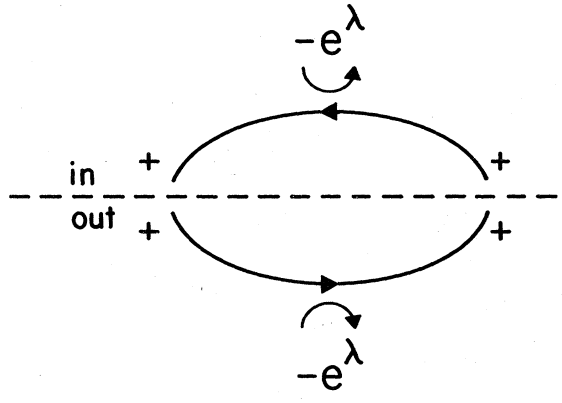

FIG. 9. Loop involving chiral switch.

Further contributions which are now being studied involving both chiral and so-called color switches but still corresponding to planar-type analyticity will not only shift the trajectories in Fig. 6 but will also reorder the trajectories and split the mass degeneracy. Results on this problem will be reported elsewhere.

The requirement of the Froissart bound does apply to the scalar function f but this will happen automatically since the leading trajectory in f is the lowest trajectory in Fig. 6, $\alpha_0(s)$, and clearly $\alpha_0(0) < 1$.

ACKNOWLEDGMENTS

This work was supported in part by National Science Foundation Grant No. PHY-8308053. We thank Professor Paul Finkler for helpful discussions.

[1]G. F. Chew and C. Rosenzweig, Phys. Rep. **41C**, 263 (1978).
[2]G. F. Chew and V. Poenaru, Z. Phys. C **11**, 59 (1981).
[3]G. F. Chew and M. Levinson, Z. Phys. C **20**, 19 (1983).
[4]See, for example, P. Gauron, B. Nicolescu, and S. Ouvry, Phys. Rev. D **24**, 2501 (1981).
[5]C. E. Jones and J. Uschersohn, Phys. Rev. D **27**, 366 (1983).
[6]See Ref. 2, and G. F. Chew and J. Finkelstein, Z. Phys. C **13**, 161 (1982).
[7]H. P. Stapp, D **27**, 2445 (1983); **27**, 2478 (1983). See also Ref. 5.
[8]A. D. Martin and T. D. Spearman, *Elementary Particle Theory* (North-Holland, Amsterdam, 1970).
[9]C. E. Jones and P. Finkler, Phys. Rev. D **31**, 1393 (1985).
[10]L. A. P. Balazs, P. Gauron, and B. Nicolescu, Phys. Rev. D **29**, 533 (1984).